




Global transformer overheating from geomagnetic storms

Morgan Rivers  and Lukasz G. Gajewski 
*Alliance to Feed the Earth in Disasters (ALLFED),
603 S. Public Rd #57 Lafayette, CO 80026, USA**

David Denkenberger 
*Alliance to Feed the Earth in Disasters (ALLFED),
603 S. Public Rd #57 Lafayette, CO 80026, USA* and*

Department of Mechanical Engineering, University of Canterbury, Christchurch, Canterbury 8041, NZ

Geomagnetic storms occurring due to sustained, high-speed solar winds are known to induce currents in power distribution networks. These geomagnetically induced currents (GICs) can cause high voltage transformers (HVT) to overheat, thus resulting in a catastrophic electricity loss (CEL). Since significant portions of infrastructures around the world rely heavily on access to electric power, it is essential to estimate the risks associated with GICs on a global scale. We assemble multiple methodologies across various scientific disciplines to develop a framework assessing the probability of a severe geomagnetic storm causing a long-term, widespread power outage. Our model incorporates thermal models of HVT tie bar hot spots, historical geoelectric field estimates, and a global conductivity model to estimate the risk of long-term power outage for regions between -70° and 80° geomagnetic latitude due to transformer overheating failure. Assuming a uniform 33% HVT spare capacity, our analysis indicates that a 1 in 10,000 year storm would result in approximately 1% of the population in Europe and North America experiencing a long-term (months to years) electricity loss.

Keywords: geomagnetic storms, power grid resilience, catastrophic electricity loss, critical infrastructure, interdisciplinary systems modelling, global catastrophic risk

I. INTRODUCTION

The phenomenon known as the geomagnetic storms has been studied for hundreds of years[1], but only recently, due to advances in electrification, some are starting to worry about the potential risks they can pose to our society [2, 3]. A society that is increasingly dependent on electricity and related technologies [2, 4]. Geomagnetic storms result from an energy exchange from the solar wind into Earth’s magnetosphere. They are triggered by sustained periods of high-speed solar wind, and the most significant storms involve solar coronal mass ejections (CMEs) [5]. CMEs are the largest-scale eruptive phenomenon in the solar system – the bulk of plasma with a mass of 10^{13} kg is hauled up out to the interplanetary space with a velocity of more than 1000 km/s [6]. These storms induce intense currents in Earth’s magnetosphere, affecting the radiation belts, ionosphere, and thermosphere. We typically measure them by indices such as the disturbance storm time – Dst – and a planetary geomagnetic disturbance index – Kp [7]. The consequences include increased atmospheric density affecting satellite orbits, disruptions to navigation systems like GPS, and the generation of harmful geomagnetic induced currents (GICs) in power grids. These extreme events can also be visually stunning in the form of aurorae, such as the commonly known northern lights, despite their potentially disruptive nature [8].

GICs are what they sound like – electric currents that appear (are induced) in, e.g., power lines as a consequence of rapid changes in Earth’s magnetic field, and those currents can be a cause of worry for the stability and health of power distribution networks [9].

This worry about GICs mainly consists of two phenomena: overheating components (predominantly transformers) and tripping safety switches causing cascade failures [10]. The jury on whether these constitute a significant societal risk is still out. Scientific studies on this issue are mostly localised (i.e., consider one particular region instead of all of the Earth), and severity claims vary from no risk at all [11, 12] to catastrophic, such as trillions of dollars in damages and years of recovery [13–15], with most ending somewhere in between [10, 16–20]. It is worth noting that while the global risk of GICs is still undetermined, there are documented cases of damage to power grids from GICs [19, 20], including severe cases like the Quebec power failure of 1989 [21]. The problem with assessing the risk here is that strong enough events to cause damage are exceedingly rare, and a replay of the largest documented case from 1859, commonly referred to as the Carrington event[22], is yet to be seen.

For further reading on this topic, we refer the Reader to [10, 18, 21] and references therein.

Since there seems to be a gap in the body of literature dealing with widespread events reaching global scales, we attempt to partially fill this gap in this paper. Even though our analysis here shall be limited to Europe and North America due to limits in data availability, we develop a methodology to assess the consequences of various strengths of geomagnetic storms on a global scale.

* morgan@allfed.info

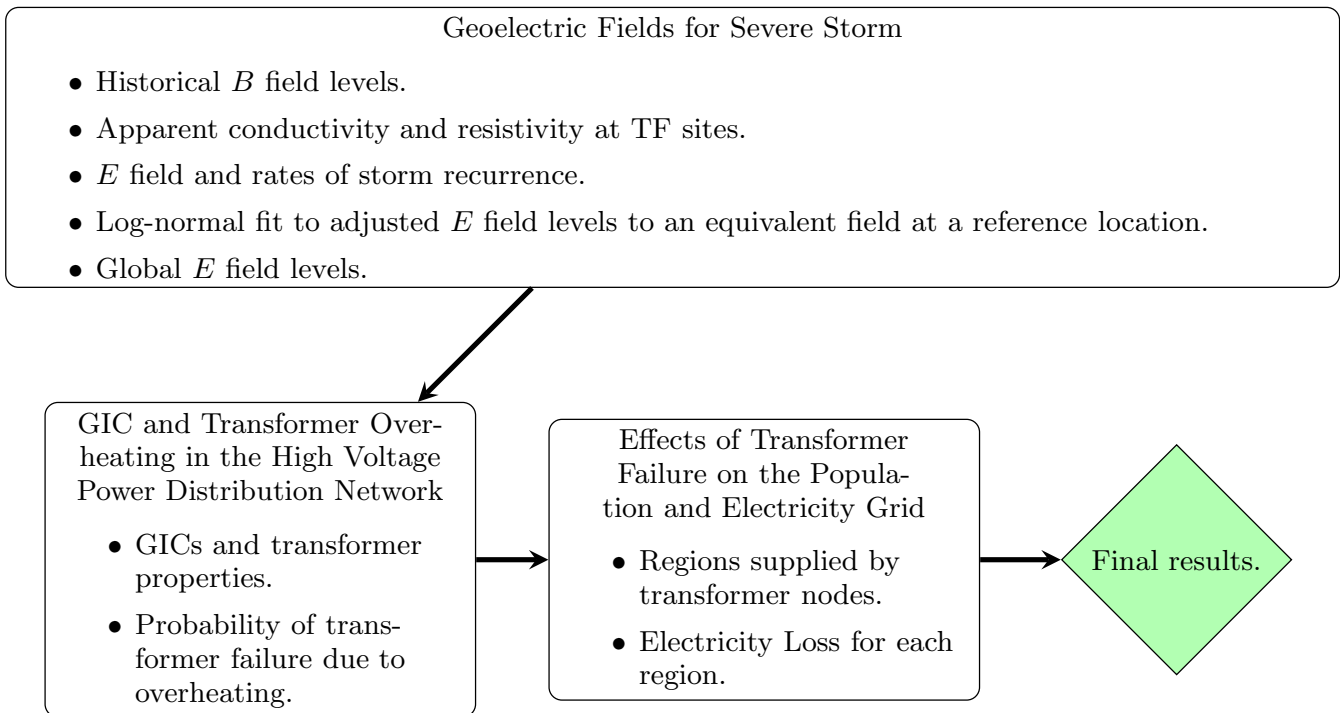


FIG. 1. Simplified flowchart of our proposed framework. The general model consists of three main stages and results in concrete estimates of regional power outages for arbitrary locations on Earth and how those outages affect the population. A detailed flowchart is available along with the model’s source code at <https://github.com/allfed/GeomagneticModel>.

The framework can be applied to any geographical region where the power grid is known with sufficient accuracy and completeness. The software implementation of our model is open-source[23], written in Python, and can be run on a modern PC without the need for a computing cluster or a super-computer.

In this article, we specifically tackle the issue of overheating transformers in power grids due to GICs on an international scale, utilising data from global magnetic field observation (MT) stations [24], electromagnetic transfer function (EMTF) repository [25–27], crowd-sourced power distribution network [28] as well as OpenStreetMap [29], North American Electric Reliability Corporation (NERC) [30, 31], and Electric Power Research Institute (EPRI) [32–35]. In order to assess the effect on population, we used data from the U.S. Energy Information Administration, and the Center for International Earth Science Information Network, Columbia University [36–38].

Our primary target is estimating the population numbers experiencing a catastrophic electricity loss (CEL) given a recurrence class of a geomagnetic storm (e.g., a 1 in 100 year event).

II. METHODS

In Fig. 1, we present a simplified flowchart of our model (a full picture is available in the source code repository:

<https://github.com/allfed/GeomagneticModel>). We partition the model into three distinct stages, described in detail as follows.

A. Stage I

This stage is based on the methodology developed by Love et al., [39] and consists of estimating historical magnetic field – B – levels, determining apparent conductivity and resistivity at electromagnetic transfer function sites (EMTF or TF, for short), calculating electric field – E – levels at magnetotelluric (MT) stations and recurrence rates for those levels, adjusting E field levels to a reference location, and finally computing E fields around the globe from the adjusted E fields.

MT stations have been measuring the B field regularly for many decades. Through these data, we are able to determine the statistics on the recurrence of E fields over a long period and thus forecast the repeat rates of the less frequent, larger amplitude events. We obtained the data at the Fresno, California, USA MT site (FRN) from the global ground-based magnetometer initiative (SuperMAG) [24]. These data contain measurements of the magnetic field every minute for 37 years ending in 2019. It is worth noting that the results presented here depend on the choice of the site due to inaccuracies in the apparent conductivity model. The FRN dataset was picked because of its proximity to an EMTF site (RET06), suf-

ficient data size, and time span. For more precise results, data from all existing MT and EMTF sites would need to be combined into one dataset or a better apparent conductivity model established, ideally both; however, this falls out of the scope of this paper.

We then process this dataset as described in [39] Sec. 5: the time series of B is detrended by subtracting a second-order polynomial fitted to the entire duration of the time series, and any missing data are filled by linear interpolation. Then, the series is put through a fast Fourier transform (FFT), multiplied by an appropriate transfer tensor for the survey site, and finally, a reverse FFT is performed, resulting in a geoelectric $-E-$ series. This procedure is rooted in the relationship between the geomagnetic and geoelectric fields at the Earth's surface: [40, 41]

$$\mathbf{E}(f, x, y) = \frac{1}{\mu} \mathbf{Z}(f, x, y) \cdot \mathbf{B}(f, x, y), \quad (1)$$

where f is the frequency of sinusoidal variation, x and y are horizontal Cartesian components, μ is permeability, and \mathbf{Z} is the impedance tensor specifying the amplitude, polarisation and phase of the geoelectric field. The transfer tensor mentioned earlier is \mathbf{Z}/μ .

In order to compute E fields using Eq.(1) we need to determine the apparent conductivity and resistivity at the corresponding TF site. We acquire the necessary data from the SPUD EMTF repository [25–27] at the Dog Creek, California, USA site (RET06) corresponding to the chosen MT site in Fresno. The apparent conductivity can be expressed as: [39]

$$\sigma_A(f) = \frac{2\pi\mu f}{|\mathbf{Z}(f)|^2}, \quad (2)$$

where $|\cdot|$ is the Frobenius norm[40], and the apparent resistivity is given by: [40, 42]

$$\rho(f) = \frac{|\mathbf{Z}(f)|_{\odot}^2}{2\pi\mu f}, \quad (3)$$

where $|\cdot|_{\odot}$ represents an element-wise norm.

With E fields established, we now consider an adjustment coefficient that describes the relationship between fields' strengths and durations (SI Fig. S1). The peak electric field levels that occur once every ten years change with the duration over which they are sustained; namely, longer duration corresponds to lower peak field levels. Thus, we compare the mean field level lasting sixty seconds to longer-lasting fields. We shall use this adjustment later to predict the strength of GICs in transformers to ensure we do not overestimate the current levels of long-duration GICs.

Our ultimate goal of this stage is to compute E fields (their strength and occurrence rates) at an arbitrary location on Earth, extrapolating from the measurement site. For this purpose, we adjust all measured fields to an arbitrarily chosen reference with conductivity $\sigma_{ref} =$

$8.7 * 10^{-6}[\frac{S}{m}]$, located at a magnetic latitude $L_M = 72^\circ$ N so that we can model E fields globally with a single function regardless of the choice of the MT site or even ensemble of sites. To this end, we incorporate an auroral boundary shift using an estimated auroral boundary movement of 0.004 degrees threshold shift south per [nT] Dst as per the recommendation in the report from EPRI [32], with the Dst estimates taken from Oughton et al., [18]. Subsequently, we use the geomagnetic latitude distribution data from Ngwira et al.,[43] to compute a magnetic latitude adjustment \hat{L}_M , and we establish the apparent conductivity adjustment as $\hat{\sigma}_A = \sigma_A/\sigma_A^{ref}$.

Thus, we obtain a formula for the reference E field:

$$|E_{ref}| = \hat{L}_M \hat{\sigma}_A |E|. \quad (4)$$

We can now fit a log-normal function to all E field data (SI Fig. S2) and then use this model to estimate geoelectric fields at an arbitrary point on Earth [39, 44].

This arbitrary location E field estimation is conducted with the help of Earth's ground conductivity at a 15 arc-minute basis from Alekseev et al., [45]. It is a layered model, so we calculate the impedance recursively as prescribed in the NERC report [31]. Finally, we adjust the E field at the reference site back to the expected field levels for all points on Earth at 15 arc-minute resolution via:

$$|E| = \frac{1}{\hat{L}_M \hat{\sigma}_A} |E_{ref}|. \quad (5)$$

This concludes stage one, and in Fig. 2, we present our prediction for the expected peak magnitude of a sixty-second E field in a 1-in-100 year storm for Europe and North America.

B. Stage II

In this stage, we determine the GICs in power grids and, thus, the transformer failure due to overheating. We gathered the worldwide power distribution network data from OpenGridMap [28]. It is an open-source initiative that utilises crowd-sourced data to automatically generate power grid models in a Common Information Model (CIM) format, which is the power industry standard [46]. Since we focus in this paper on high voltage networks and high voltage transformers (HVT), we selected all lines above 100 [kV]. As pointed out in the introduction, we will be restricting ourselves to only two continents, and the primary reason for this is data availability (or lack thereof) in the OpenGridMap. We present plots of the selected networks in SI Fig. S3.

On these grids, the GICs were computed with the help of the open-source package – GEOMAGICA [47], which implements the Lehtinen-Pirjola method [48] for the Austrian grid. We modified this code such that it can be applied to an arbitrary location on Earth. Each power line length was preserved accurately, and the full length of the

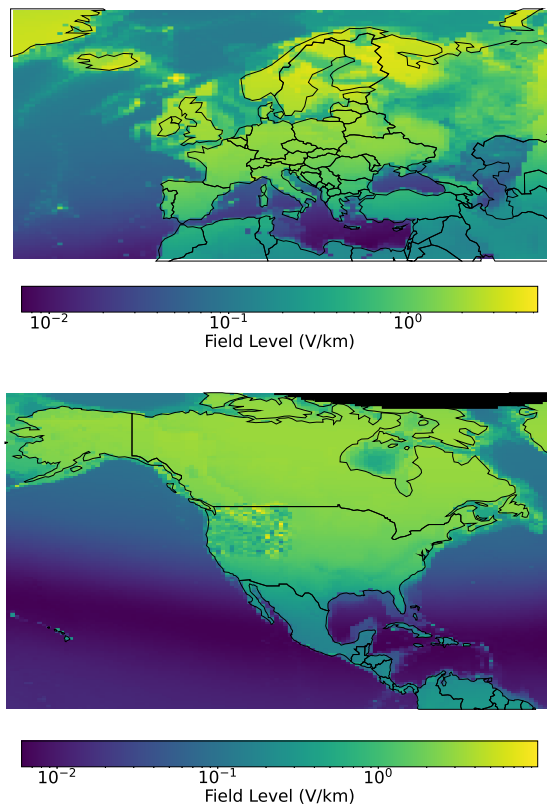


FIG. 2. Peak 60-second geoelectric field magnitude for a 1-in-100 year storm in Europe (top) and North America (bottom). The colour indicates the field level [V/km].

line was used to estimate overall line resistance; however, the GEOMAGICA package only allows for straight line estimates of induced GIC. The resistance per kilometre, as well as HVT winding conductance, were estimated using linear interpolation of line conductance as a function of AC voltage using values provided in a NERC report [30], with the ground resistance being set to $0.5[\Omega]$.

Final GIC per phase values for transformers were estimated as the expected GIC per phase flowing through the ground grid divided by 1.3. This factor brings the final values closer to those obtained with more complex transformer circuit configurations and is discussed in further detail in [18]. The absolute values of geoelectric fields were applied uniformly in the East-West direction, as this is the primary field orientation [49, 50]. If the GIC duration is longer than a minute, we scale its magnitude down to account for the decreasing statistical likelihood of an E field sustained for a longer duration (as explained in stage one, also see, SI Fig. S1), and the fact that GICs are proportional to the electric field $I_{GI} \propto E$.

With GIC levels and their recurrence rates established, we move on to determine whether they cause sufficient heat increase in transformers to result in transformer failure. We source the steady state temperature rise $T^*(I_{GI})$ for 42 different types of transformers and two tie bar ge-

ometries from an EPRI report [34] and linearly interpolate the data where necessary, as well as the temperature response for both designs – τ . These data were extracted by hand from the said report. Both T^* and τ are multiplied by $\frac{2}{3}$ to accommodate the fact that the studied tie bar geometry designs represent the extreme “best” and “worst” cases; thus, we are considering the midpoint between them (this scaling factor can be found via inspecting the EPRI report). The HVT temperature can be found as: [33]

$$T_{HVT} = T^*(I_{GI}) \left(1 - e^{-\frac{t}{\tau}}\right) + T_{oil}, \quad (6)$$

where t is the duration, and $T_{oil} = 90^\circ C$ is the surface oil temperature assumed in a severe geomagnetic storm [34].

To determine whether the temperature in Eq. (6) makes a transformer fail, we look at the structural temperature limit in [33], which is a function of the transformer’s age. We estimate the transformer population age distribution based on the statistics in the same report. Each transformer has an associated voltage class (V_c), which we assign based on the proximity to one of $\{230, 345, 500, 765\}$ [kV]. These values are chosen specifically as these have associated statistics on the transformer phase demographics in the aforementioned report and prevalence in the US grid per class [35]. The US dataset was the easiest to obtain, and we assume grids around the world would not have significantly different characteristics in these particular features. However, should that not be the case, it is fairly straightforward to substitute this number for a region-specific one if needed (for those who have access to the data). We use the cumulative fraction of transformer population exceeding safe temperatures as the proxy for the probability of failure for the transformer in a given class; therefore, we can write:

$$F(V_c) = f(V_c) \sum_A f(T_{HVT} > T_{max}) f(A), \quad (7)$$

where $F(V_c)$ is the fraction of transformers overheating in class V_c , A is the age category, with $f(A)$ the fraction of transformers in given age category, and $f(T_{HVT} > T_{max})$ is the fraction of transformers above safe temperature for the age, and $f(V_c)$ is the fraction associated with the transformer type. For each of the 42 transformer types, we associate V_c and a phase ϕ with them, and now, each transformer is a member of a group. E.g., there are seven types in a group defined by $\{V_c = 500, \phi = 1\}$, so for each transformer in this group, $f(V_c) = 1/7$. All the values for transformer types, temperature limits, and transformer population are presented in SI Table S1, S2, and S3.

Ultimately, we want to assess whether a power network node n fails, and we achieve that by estimating the percentage of transformers failing at any given node as:

$$F(n) = \sum_{\{\phi, V_c\}} \left(f(\phi) f_{grid}(V_c) \sum_{V_c} F(V_c) \right). \quad (8)$$



FIG. 3. European substations at risk of electricity loss after a 1-in-10000 year storm. Colour indicates the fraction of HVTs we expect to fail within a given Voronoi tile.

$f_{grid}(V_c)$ is the prevalence of transformers in class V_c in the power grid, and $f(\phi)$ is the fraction of transformers with phase ϕ . If $F(n) > 0.33$, then we conclude that node n fails longer term. This cutoff value is based on the report for Oak Ridge National Laboratory[51], in which we can find that “*the standard approach to spares has been to purchase an extra single phase transformer for a three phase bank*”. Thus, we assume that if the failure rate is more than 33% in a given region, the region suffers an extended power outage.

C. Stage III

We conclude how transformer failures affect population access to electricity. Our consideration here is based on the tessellation of the continents. It could also be performed in countries and alike, but we focus on continents in the analysis. Unfortunately, the region served by each substation node is not publicly available, so we use a proxy approach – a Voronoi diagram. Each power grid node in the power distribution data serves as the centre for a Voronoi cell. This way, we have a good approximation of real-world electric districts since each power substation serves its nearest surroundings. Naturally, we limit the Voronoi regions to the extent of the geographic boundaries of the networks. We use the 15 arc-minute grid population density data to estimate the population in each cell [37]. Specifically, in each grid cell, the land area was multiplied by the population density to obtain

the absolute population estimates. The total population in each Voronoi region was calculated as the total number of centres of 15 arc-minute population grid cells within the Voronoi polygon represented by a power node.

We assume the power outages to be long-term as the grid is often run at near-maximum capacity, and it is estimated that a region with insufficient transformers would be unable to serve electricity for many months until those transformers were replaced, which is a slow and expensive process. This is a lower bound estimate, however, and could well take much longer [51].

In addition to the number of people being cut off from power, we provide estimates on the total electric power loss in [GW]:

$$P_{loss} = \frac{P_{cons}}{N} \sum_n C(n) [F(n) > 0.33]. \quad (9)$$

P_{loss} is power lost, P_{cons} is total power consumption (for continent/country, etc.) [38], N is total population [36], $C(n)$ is the population in a given Voronoi region n , $F(n)$ is from Eq. (8), and $[\dots]$ is the Iverson bracket notation.

III. RESULTS AND DISCUSSION

To recap, In Fig. 1, we presented a simplified flowchart of our model. The data-driven framework we propose runs in three stages estimating: 1) geoelectric fields for severe storms, 2) GICs and transformer overheating in

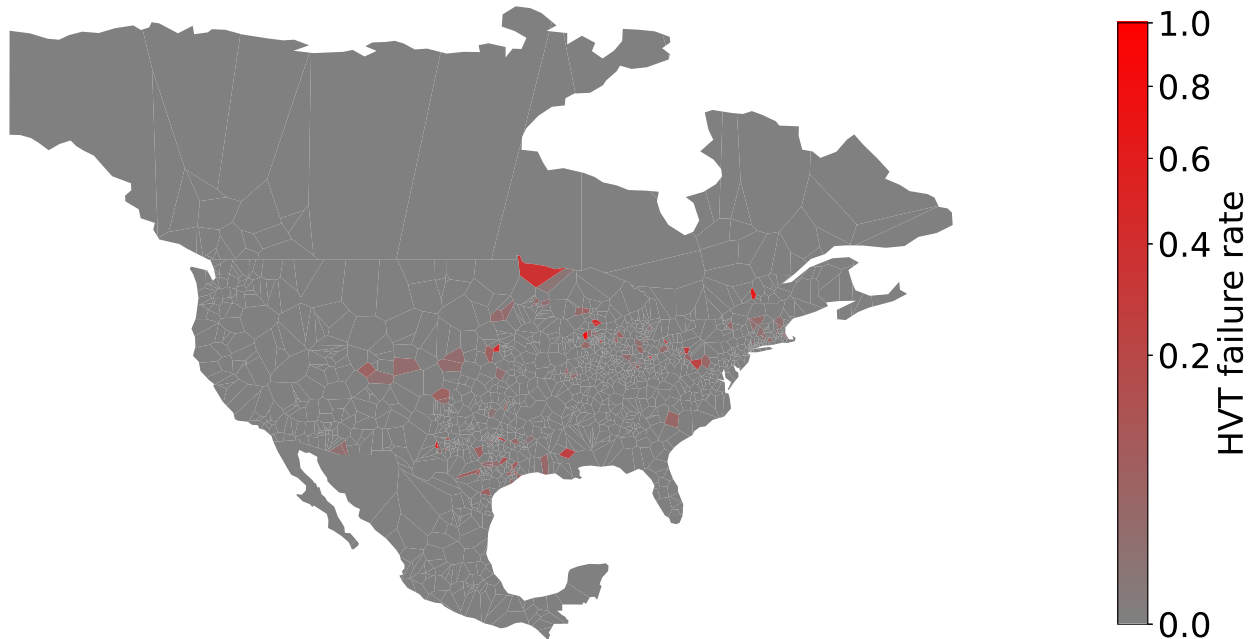


FIG. 4. North American substations at risk of electricity loss after a 1-in-10000 year storm. Colour indicates the fraction of HVTs we expect to fail within a given Voronoi tile.

high voltage power distribution networks, and 3) effects of transformer failure on the electric grid and population's access to electricity. This three-stage process is an agglomeration of multiple smaller models we assembled across various scientific fields and modified or expanded where appropriate to suit our needs.

We utilise magnetotelluric (MT) [24] and EMTF [25–27] site data to find geoelectric fields as described by Love et al., [39]. Then, an adjustment process is applied to all fields to a reference location, with an intermediary step incorporating auroral boundary movement. The reference adjustment is done by using the geomagnetic latitude data from Ngwira et al., [43]. To this data, we fit a log-normal function that serves as our model for the recurrence of the geoelectric fields [39, 44]. Finally, an impedance estimate is computed using Earth's ground conductivity model from Alekseev et al., [45]. With all those elements, we can compute E field levels at any location on Earth for any storm rarity and duration.

This general model can be used for an arbitrary geographical region, including the whole globe, as long as power distribution network data are available. The software implementation is written in Python and the source code is open and available for anyone to use and modify. It is also worth noting that our implementation is additionally accessible to a wide audience as it does not require an expensive computer cluster, and can be run on a reasonably modern machine in less than an hour on

the scale of a continent or smaller.

In order to see how particular regions are affected by geomagnetic storms, we include the Voronoi diagram plots for both continents depicting a specific number of substations at risk in a granular manner; see Fig. 3 for Europe, and Fig. 4 for North America in a 1-in-10000 year scenario. The colour indicates the ratio of HVTs within a given Voronoi cell that are expected to fail. We acknowledge that Sweden has in fact hardened their grid to address the risks discussed here [52]; however, for simplicity's sake, we include it in our results.

We determine a region to be expected to suffer a power loss by considering the transformer failures exceeding available spare parts [51]. Thus, we assume that if the failure rate is more than 33% in a given region, the region suffers an extended power outage. In Fig. 5, we present the estimates of the population numbers experiencing a CEL as a result of a geomagnetic storm, and total electricity loss in gigawatts. This plot illustrates how many people will lose power for months or perhaps even years when an extreme storm arrives. This extreme event's strength is the highest expected to occur once per certain amount of years. For instance, for an event of a strength that is expected to happen once in 10000 years, in Europe, we expect 0.99% (over 7.4 million people) of the population to experience CEL, whereas in North America, it would be 0.86% (over 4.1 million people). The total expected loss is 49.71 [GW] and 56.12 [GW], re-

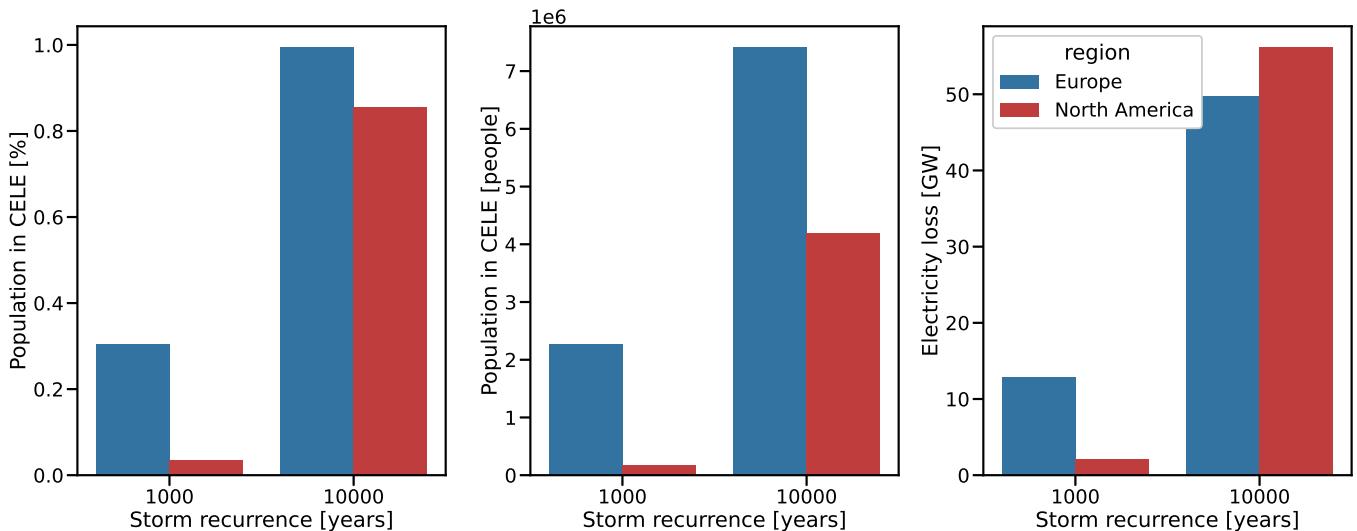


FIG. 5. Population volume experiencing CEL as a function of storm rarity in [%] (left), the number of people (centre), and electricity loss in gigawatts (right).

spectively. We limited ourselves here to these particular metrics, but of course, this analysis can be expanded to include the expected loss of GDP, industry production, and so on.

Geomagnetically induced currents are a serious cause for concern, considering how reliant many of humanity’s critical infrastructure systems are on electric power [53]. While plenty of papers tackle this issue in a localised and narrow manner, to our knowledge, no attempt at a global risk analysis has been conducted. We tackle the problem of filling this knowledge gap and develop a general model that combines all adequate specific methods from thermal models of HVT tie bar hot spots through historical geoelectric field estimates to a global conductivity model. It is our belief that the methodology presented in this paper can be applied on a global scale and inform the decisions of policymakers in regulating power distribution network resilience.

Our main analysis was limited to only two continents – Europe and North America – due to a lack of quality data in other regions; however, these two serve as very good proofs of concept. The key results show that a severe geomagnetic storm can severely affect millions of people. We believe that rather than approaching our results as final, they should be considered as a starting point for further analysis and a powerful tool and framework for future work, where more accurate grid connections, transformer designs and voltages, grounding resistances, and other specifics on a global scale can be used to obtain realistic results for a given region. The unpredictable and rare nature of coronal mass ejections impacting Earth makes the risk assessment much more difficult since, at the time of writing this manuscript, it is virtually impossible to say what precisely the chances of a 1-in-10000 year storm occurring within the next decade are. While it seems prudent and most likely cost-effective to prepare

the grid for severe storms instead of waiting for failures to happen, a global-scale complete power outage does not seem possible with the assumptions we have made in our model.

With that said, the data we have used to predict HVT overheating is limited. Our grid model relies on potentially incomplete or incorrect infrastructure data crowdsourced by OpenStreetMaps, due to the lack of official public high voltage infrastructure data. However, this does not represent a failure of the model, as electrical utilities and government agencies can readily replace our grid map with their own private data for enhanced prediction accuracy.

One could potentially adapt our model to use a characteristic power line length or a synthetic network instead of real data, but this leads to the problem of losing regional precision in predicted transformer outages. We would still have a global estimate of expected power loss, but the exact locations of predicted outages would be unreliable.

Similarly, the magnetotelluric data are still very limited, and while our method of normalising these data to a reference location and, from there, extrapolating worldwide has the advantage of universality, it does come with a drawback of potentially over-generalisation. This can lead to underestimating storm recurrence in some specific regions.

Most importantly, we only consider transformer failure due to overheating; however, the safety switch cascade failure scenario is also a very important avenue of investigation that should be explored in the future, as well as other more complex interactions with the increasingly complex digital infrastructure automatically routing power through the electrical grid.

Overall, to our knowledge, the approach proposed in this paper is the first of its kind in assessing power distri-

bution network resilience to GICs and can be broadly applied at municipality, country, continent or even a global level to inform governing bodies and private entities alike of the dangers associated with transformer overheating during geomagnetic storms.

DISCLOSURE STATEMENT

Authors report that there are no competing interests to declare.

DATA AVAILABILITY STATEMENT

All data used in this research are publicly available. The program source code and instructions on how to procure the data can be found in the github repository of the project: <https://github.com/allfed/GeomagneticModel>.

-
- [1] G. S. Lakhina and B. T. Tsurutani, Geomagnetic storms: historical perspective to modern view, *Geoscience Letters* **3**, 1 (2016).
- [2] J. F. Organek, Black sky hazards: Resilience planning, in *Congress on Technical Advancement 2017* (2017) pp. 29–40.
- [3] K. Schulz, What a Major Solar Storm Could Do to Our Planet, <https://www.newyorker.com/magazine/2024/03/04/what-a-major-solar-storm-could-do-to-our-planet> (2024), accessed: 2024-03-05.
- [4] L. Löfquist, Is there a universal human right to electricity?, *The International Journal of Human Rights* **24**, 711 (2020).
- [5] J. T. Gosling, The solar flare myth, *Journal of Geophysical Research: Space Physics* **98**, 18937 (1993).
- [6] P. Chen, Coronal mass ejections: models and their observational basis, *Living Reviews in Solar Physics* **8**, 1 (2011).
- [7] W. Gonzalez, J.-A. Joselyn, Y. Kamide, H. W. Kroehl, G. Rostoker, B. T. Tsurutani, and V. Vasyliunas, What is a geomagnetic storm?, *Journal of Geophysical Research: Space Physics* **99**, 5771 (1994).
- [8] Geomagnetic Storms, <https://www.swpc.noaa.gov/phenomena/geomagnetic-storms> (2014), accessed: 2023-11-24.
- [9] A. Pulkkinen, E. Bernabeu, A. Thomson, A. Viljanen, R. Pirjola, D. Boteler, J. Eichner, P. Cilliers, D. Welling, N. Savani, *et al.*, Geomagnetically induced currents: Science, engineering, and applications readiness, *Space weather* **15**, 828 (2017).
- [10] D. Roodman, The risk of geomagnetic storms to the grid: A preliminary review, Available at SSRN 3635861 (2015).
- [11] M. Švanda, A. Smičková, and T. Vřboš'oková, Modelling of geomagnetically induced currents in the Czech transmission grid, *Earth, Planets and Space* **73**, 1 (2021).
- [12] R. Girgis and K. Vedante, Effects of GIC on power transformers and power systems, in *PES T&D 2012* (IEEE, 2012) pp. 1–8.
- [13] National Research Council, *Severe space weather events: understanding societal and economic impacts: a workshop report* (The National Academies Press, Washington, DC, 2008) <https://nap.nationalacademies.org/catalog/12507/severe-space-weather-events-understanding-societal-and-economic-impacts-a>.
- [14] C. Said, Everything I've learned about solar storm risk and EMP attacks, <https://chris-said.io/2020/06/18/everything-ive-learned-about-solar-storm-risk-and-emp-attacks/> (2020), accessed: 2023-11-24.
- [15] M. Weiss and M. Weiss, An assessment of threats to the American power grid, *Energy, Sustainability and Society* **9**, 1 (2019).
- [16] J. M. Torta, S. Marsal, and M. Quintana, Assessing the hazard from geomagnetically induced currents to the entire high-voltage power network in Spain, *Earth, Planets and Space* **66**, 1 (2014).
- [17] A. Gil, M. Berendt-Marchel, R. Modzelewska, S. Moskwa, A. Siluszyk, M. Siluszyk, L. Tomasiak, A. Wawrzaszek, and A. Wawrzynczak, Evaluating the relationship between strong geomagnetic storms and electric grid failures in Poland using the geoelectric field as a GIC proxy, *Journal of Space Weather and Space Climate* **11**, 30 (2021).
- [18] E. J. Oughton, M. Hapgood, G. S. Richardson, C. D. Began, A. W. P. Thomson, M. Gibbs, C. Burnett, C. T. Gaunt, M. Trichas, R. Dada, and R. B. Horne, A Risk Assessment Framework for the Socioeconomic Impacts of Electricity Transmission Infrastructure Failure Due to Space Weather: An Application to the United Kingdom, *Risk Analysis* **39**, 1022 (2019), <https://onlinelibrary.wiley.com/doi/pdf/10.1111/risa.13229>.
- [19] C. Gaunt and G. Coetzee, Transformer failures in regions incorrectly considered to have low GIC-risk, in *2007 IEEE Lausanne power tech* (IEEE, 2007) pp. 807–812.
- [20] N. Moodley and C. Gaunt, Developing a power transformer low energy degradation assessment triangle, in *IEEE Power and Energy Society Conference and Exposition in Africa: Intelligent Grid Integration of Renewable Energy Resources (PowerAfrica)* (IEEE, 2012) pp. 1–6.
- [21] C. Gaunt, Why space weather is relevant to electrical power systems, *Space Weather* **14**, 2 (2016).
- [22] B. T. Tsurutani, W. D. Gonzalez, G. Lakhina, and S. Alex, The extreme magnetic storm of 1–2 September 1859, *Journal of Geophysical Research: Space Physics* **108** (2003).
- [23] <https://github.com/allfed/GeomagneticModel>.
- [24] J. Gjerloev, A global ground-based magnetometer initiative, *Eos, Transactions American Geophysical Union* **90**, 230 (2009), <https://supermag.jhuapl.edu/>. Accessed: 2023-12-11.
- [25] A. Kelbert, G. Egbert, and A. Schultz, IRIS DMC data services products: EMTF, the magnetotelluric transfer functions, National Geoelectromagnetic Facility Technical Report (2011).

- [26] A. Kelbert, Taking magnetotelluric data out of the drawer, in *AGU Fall Meeting Abstracts*, Vol. 2019 (2019) pp. IN21A-01, <https://ds.iris.edu/spud/emtf>. Accessed: 2023-12-11.
- [27] A. Kelbert, P. A. Bedrosian, and B. S. Murphy, The first 3D conductivity model of the contiguous United States: Reflections on geologic structure and application to induction hazards, Geomagnetically induced currents from the Sun to the power grid, 127 (2019).
- [28] J. Rivera, J. Leimhofer, and H.-A. Jacobsen, OpenGridMap: towards automatic power grid simulation model generation from crowdsourced data, *Computer Science-Research and Development* **32**, 13 (2017), <https://github.com/OpenGridMap/transnet-models>. Accessed: 2023-12-11.
- [29] OpenStreetMap contributors, Region extent data retrieved from <https://download.geofabrik.de/>, <https://www.openstreetmap.org> (2017), accessed: 2023-12-13.
- [30] North American Electric Reliability Corporation (NERC), Network applicability, project 2013-03, EOP-010-1, <https://www.nerc.com/pa/Stand/Project201303GeomagneticDisturbanceMitigation/ApplicableNetwork.pdf> (2013), accessed: 2023-12-11.
- [31] North American Electric Reliability Corporation (NERC), Computing geomagnetically-induced current in the bulk-power system, https://www.nerc.com/comm/PC/Geomagnetic%20Disturbance%20Task%20Force%20GMDTF%202013/GIC%20Application%20Guide%202013_approved.pdf (2013), accessed: 2023-12-12.
- [32] Electric Power Research Institute (EPRI), Palo Alto, CA: 2020. 3002017952., Magnetohydrodynamic (MHD) modeling for the further understanding of geoelectric field enhancements and auroral behavior during geomagnetic disturbance events, <https://www.epri.com/research/products/000000003002017952> (2020), accessed: 2023-12-12.
- [33] Electric Power Research Institute (EPRI), EPRI, Palo Alto, CA: 2017. 3002009001, Magnetohydrodynamic electromagnetic pulse assessment of the continental U.S. electric grid: Geomagnetically induced current and transformer thermal analysis, <https://ed-thelen.org/pics/EPRI-HEMP-2017.pdf> (2017), accessed: 2023-12-12.
- [34] Electric Power Research Institute (EPRI), Palo Alto, CA: 2019. 3002017708., Transformer thermal impact assessments for dc withstand capability: Examining the impacts of geomagnetically induced current (GIC) on transformer thermal performance, <https://www.epri.com/research/products/000000003002017708> (2019), accessed: 2023-12-12.
- [35] J. G. Kappenman and B. W. McConnell, Meta-R-322 Low-Frequency Protection Concepts for the Electric Power Grid: Geomagnetically Induced Current (GIC) and E 3 HEMP Mitigation, Metatech Corporation, 358 S. Fairview Ave., Suite E, Goleta, CA 93117 <https://api.semanticscholar.org/CorpusID:62781689> (2010).
- [36] U.S. Energy Information Administration, Population by country, <https://www.eia.gov/international/data/world/other-statistics/population-by-country> (2020), accessed: 2023-12-13.
- [37] Center for International Earth Science Information Network - CIESIN - Columbia University, Gridded Population of the World, Version 4 (GPWv4): Population Density, Palisades, New York: NASA Socioeconomic Data and Applications Center (SEDAC). (2020), <https://doi.org/10.7927/H49C6VHW>. Accessed: 2023-12-13.
- [38] U.S. Energy Information Administration, Electricity consumption by country, <https://www.eia.gov/international/data/world/electricity/electricity-consumption> (2020), accessed: 2023-12-13.
- [39] J. J. Love, G. M. Lucas, A. Kelbert, and P. A. Bedrosian, Geoelectric hazard maps for the Mid-Atlantic United States: 100 year extreme values and the 1989 magnetic storm, *Geophysical Research Letters* **45**, 5 (2018).
- [40] M. N. Berdichevsky and V. I. Dmitriev, *Models and methods of magnetotellurics* (Springer Science & Business Media, 2008).
- [41] A. D. Chave and A. G. Jones, *The magnetotelluric method: Theory and practice* (Cambridge University Press, 2012).
- [42] J. J. Love, G. M. Lucas, P. A. Bedrosian, and A. Kelbert, Extreme-value geoelectric amplitude and polarization across the Northeast United States, *Space weather* **17**, 379 (2019).
- [43] C. M. Ngwira, A. Pulkkinen, F. D. Wilder, and G. Crowley, Extended study of extreme geoelectric field event scenarios for geomagnetically induced current applications, *Space Weather* **11**, 121 (2013).
- [44] J. J. Love, Some experiments in extreme-value statistical modeling of magnetic superstorm intensities, *Space Weather* **18**, e2019SW002255 (2020).
- [45] D. Alekseev, A. Kuvshinov, and N. Palshin, Compilation of 3D global conductivity model of the Earth for space weather applications, *Earth, Planets and Space* **67**, 1 (2015), <https://globalconductivity.ocean.ru/>. Accessed: 2023-12-11.
- [46] J. J. Simmins, The impact of PAP 8 on the Common Information Model (CIM), in *2011 IEEE/PES Power Systems Conference and Exposition* (IEEE, 2011) pp. 1–2.
- [47] Weidelt, P. and Beggan, C. and Turnbull, A. and McKay, K. and Bailey, R., Geomagnetically induced currents in Austria (GEOMAGICA), <https://github.com/geomagpy/GEOMAGICA> (2018), accessed: 2023-12-11.
- [48] M. Lehtinen and R. J. Pirjola, Currents produced in earthed conductor networks by geomagnetically-induced electric fields, *Annales Geophysicae* **3**, 479 (1985).
- [49] T. Kikuchi, K. K. Hashimoto, and K. Nozaki, Penetration of magnetospheric electric fields to the equator during a geomagnetic storm, *Journal of Geophysical Research: Space Physics* **113** (2008).
- [50] R. Marshall, H. Gorniak, T. Van Der Walt, C. Waters, M. Sciffer, M. Miller, M. Dalzell, T. Daly, G. Pouferis, G. Hesse, *et al.*, Observations of geomagnetically induced currents in the Australian power network, *Space Weather* **11**, 6 (2013).
- [51] J. Kappenman, Meta-R-319 Geomagnetic storms and their impacts on the US power grid, Metatech Corporation, 358 S. Fairview Ave., Suite E, Goleta, CA 93117 https://www.ferc.gov/sites/default/files/2020-05/ferc_meta-r-319.pdf (2010).
- [52] E. Krausmann, E. Andersson, W. Murtagh and N. Mitchison, *Space Weather and Power Grids: Findings and Outlook. An event co-organised by the European Commission's Joint Research Centre, the Swedish Civil Contingencies Agency and the NOAA Space Weather Prediction Centre 29-30 October, 2013, Is-*

- pra, Italy*, Tech. Rep. LB-NA-26370-EN-N (Luxembourg, 2013) <https://publications.jrc.ec.europa.eu/repository/handle/JRC86658>.
- [53] J. S. Foster, E. Gjelde, W. R. Graham, R. J. Hermann, H. M. Kluepfel, R. L. Lawson, G. K. Soper, L. L. Wood, and J. B. Woodard, Report of the commission to assess the threat to the United States from electromagnetic pulse (EMP) attack, critical national infrastructures, Critical National Infrastructures (2008), <https://apps.dtic.mil/sti/pdfs/ADA484672.pdf>.

Global Transformer Overheating from
Geomagnetic Storms
Supplementary Information

Morgan Rivers and Lukasz G. Gajewski

Alliance to Feed the Earth in Disasters (ALLFED), 603 S. Public
Rd #57 Lafayette, CO 80026, USA

David Denkenberger

Alliance to Feed the Earth in Disasters (ALLFED), 603 S. Public
Rd #57 Lafayette, CO 80026, USA

Department of Mechanical Engineering, University of Canterbury,
Christchurch, Canterbury 8041, NZ

1 Methodology, stage one

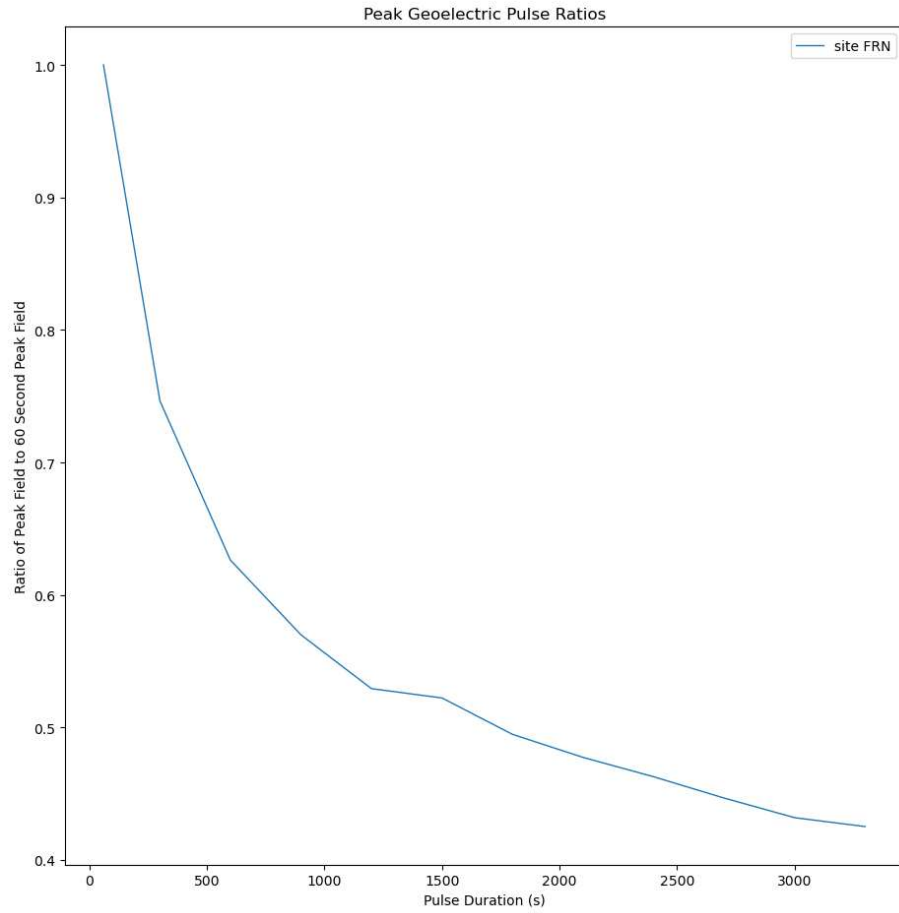


Figure 1: Peak E field level as a function of the field duration, measured at the FRN MT site. Plot shows the field level as a ratio to the field strength at 60 seconds.

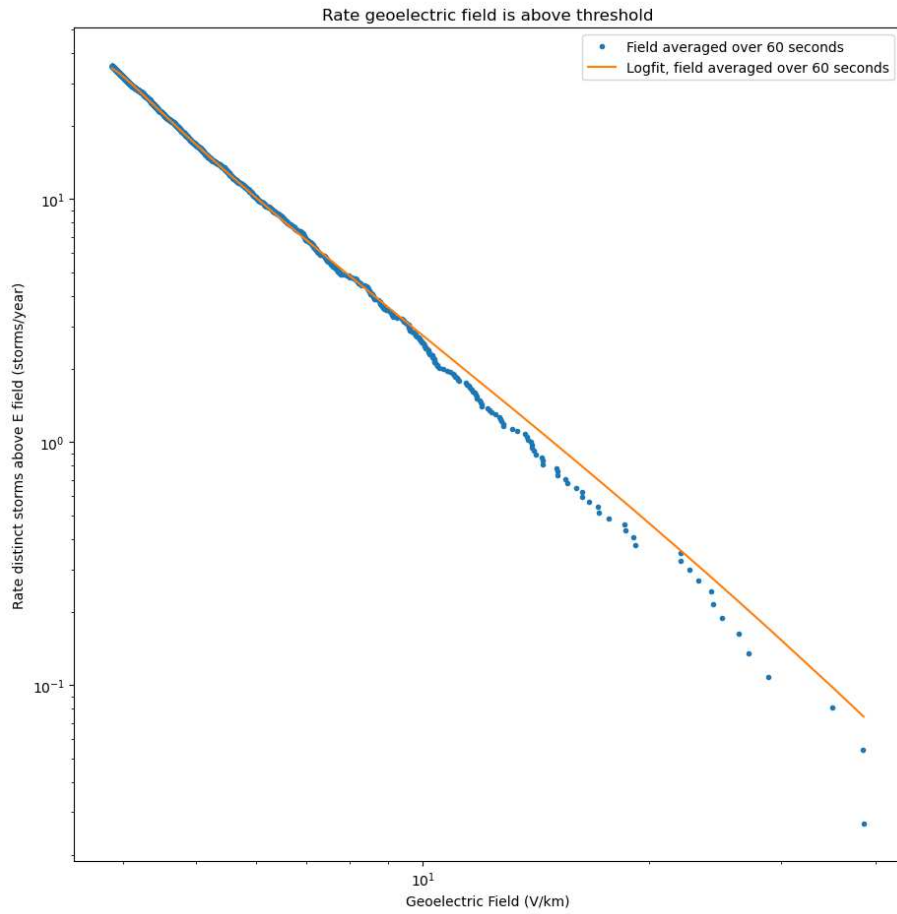


Figure 2: Normalised recurrence rates of geoelectric fields measured at the FRN MT site. This is the final result of our normalisation procedure in stage one of the method. We use the log-normal fit as per the recommendation in [1, 2].

2 Methodology, stage two

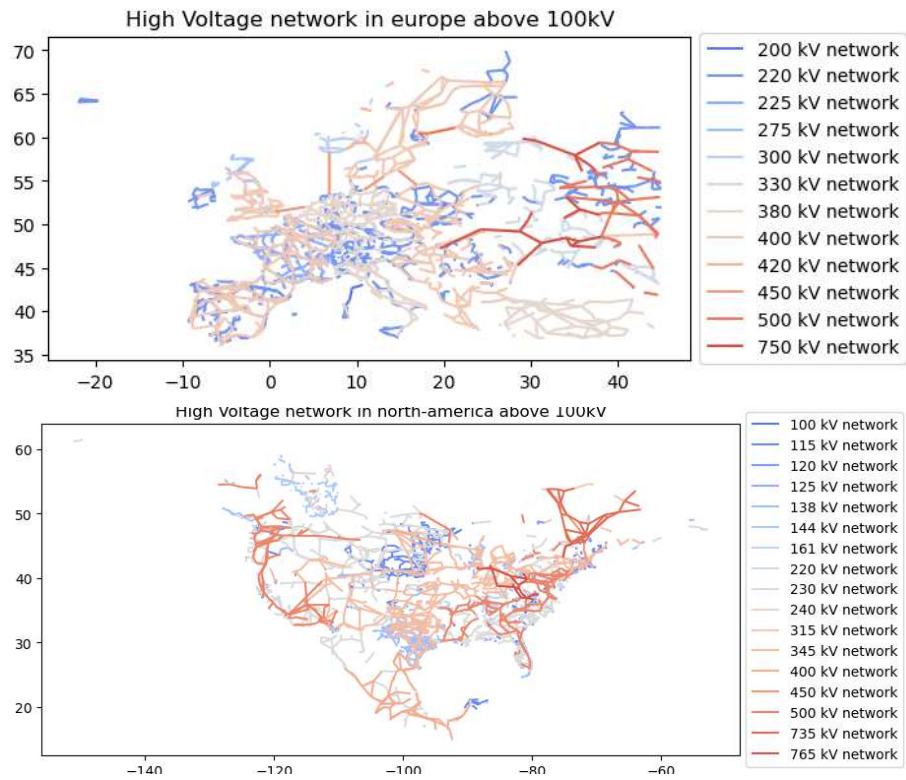


Figure 3: Power distribution networks for Europe (top) and North America (bottom) as acquired from OpenGridMap <https://github.com/OpenGridMap/transnet-models/tree/master/europe>. Only lines above 100[kV] are shown.

name	voltage	V_c	ϕ	$f(V_c)$
Tie1	526	500	single	1/7
Tie2	525	500	single	1/7
Tie3	525	500	single	1/7
Tie4	525	500	three	1/4
Tie5	525	500	three	1/4
Tie6	500	500	single	1/7
Tie7	500	500	single	1/7
Tie8	525	500	single	1/7
Tie9	500	500	three	1/4
Tie10	525	500	three	1/4
Tie11	735	765	single	1/3
Tie12	765	765	single	1/3
Tie13	746	765	single	1/3
Tie14	400	345	single	1/7
Tie15	420	345	single	1/7
Tie16	433	500	single	1/7
Tie17	410	345	single	1/7
Tie18	420	345	three	1/9
Tie19	400	345	three	1/9
Tie20	405	345	single	1/7
Tie21	405	345	three	1/9
Tie22	400	345	three	1/9
Tie23	420	345	three	1/9
Tie24	335	345	single	1/7
Tie25	345	345	single	1/7
Tie26	275	230	three	1/7
Tie27	275	230	three	1/7
Tie28	330	345	three	1/9
Tie29	345	345	single	1/7
Tie30	345	345	three	1/9
Tie31	345	345	three	1/9
Tie32	345	345	three	1/9
Tie33	230	230	single	1/5
Tie34	231	230	single	1/5
Tie35	230	230	single	1/5
Tie36	230	230	three	1/7
Tie37	230	230	three	1/7
Tie38	230	230	three	1/7
Tie39	242	230	single	1/5
Tie40	240	230	single	1/5
Tie41	225	230	three	1/7
Tie42	230	230	three	1/7

Table 1: Transformer categories. V_c is the voltage class from the main text, ϕ is phase, $f(V_c)$ is the fraction for the transformer type. Values acquired from [3].

Temp limit [$^{\circ}C$]	Age (years)	Transformer Population $f(A)$
180	0-25	0.36
160	25-40	0.25
140	> 40	0.39

Table 2: Transformer structural temperature limits per age category T_{max} and their respective prevalence as fraction of transformer population $f(A)$. Values acquired from [4].

$V_c[kV]$	Approx. Number in US Grid	$f_{grid}(V_c)$	ϕ	$f(\phi)$
230	1388	0.39	Single	0.25
230	1388	0.39	Three	0.75
345	1572	0.44	Single	0.15
345	1572	0.44	Three	0.85
500	587	0.16	Single	0.66
500	587	0.16	Three	0.34
765	58	0.01	Single	0.97 *
765	58	0.01	Three	0.03 *

Table 3: Transformer population in US grid and fractional population by phase for each voltage class. Values marked with * were rounded to the nearest integer because no 765[kV] transformers were present in the other data sets. Values acquired from [5].

References

- [1] J. J. Love, “Some experiments in extreme-value statistical modeling of magnetic superstorm intensities,” *Space Weather*, vol. 18, no. 1, p. e2019SW002255, 2020.
- [2] J. J. Love, G. M. Lucas, A. Kelbert, and P. A. Bedrosian, “Gеоelectric hazard maps for the mid-atlantic United States: 100 year extreme values and the 1989 magnetic storm,” *Geophysical Research Letters*, vol. 45, no. 1, pp. 5–14, 2018.
- [3] Electric Power Research Institute (EPRI), Palo Alto, CA: 2019. 3002017708., “Transformer thermal impact assessments for dc withstand capability: Examining the impacts of geomagnetically induced current (GIC) on transformer thermal performance.” <https://www.epri.com/research/products/000000003002017708>. Accessed: 2023-12-12.
- [4] Electric Power Research Institute (EPRI), EPRI, Palo Alto, CA: 2017. 3002009001, “Magnetohydrodynamic electromagnetic pulse assessment of the continental U.S. electric grid: Geomagnetically induced current and transformer thermal analysis.” <https://ed-thelen.org/pics/EPRI-HEMP-2017.pdf>. Accessed: 2023-12-12.
- [5] J. G. Kappenman and B. W. McConnell, “Meta-R-322 low-frequency protection concepts for the electric power grid: Geomagnetically induced current (GIC) and E 3 HEMP mitigation.” Metatech Corporation, 358 S. Fairview Ave., Suite E, Goleta, CA 93117 <https://api.semanticscholar.org/CorpusID:62781689>, 2010.